

Supporting Information for “Unmixing river sediments for the elemental geochemistry of their source regions”

Alex G. Lipp¹, Gareth G. Roberts¹, Alexander C. Whittaker¹,

Charles J. B. Gowing², Victoria M. Fernandes¹

¹Department of Earth Sciences and Engineering, Imperial College London, UK

²Centre for Environmental Geochemistry, British Geological Survey, Keyworth, UK

Contents of this file

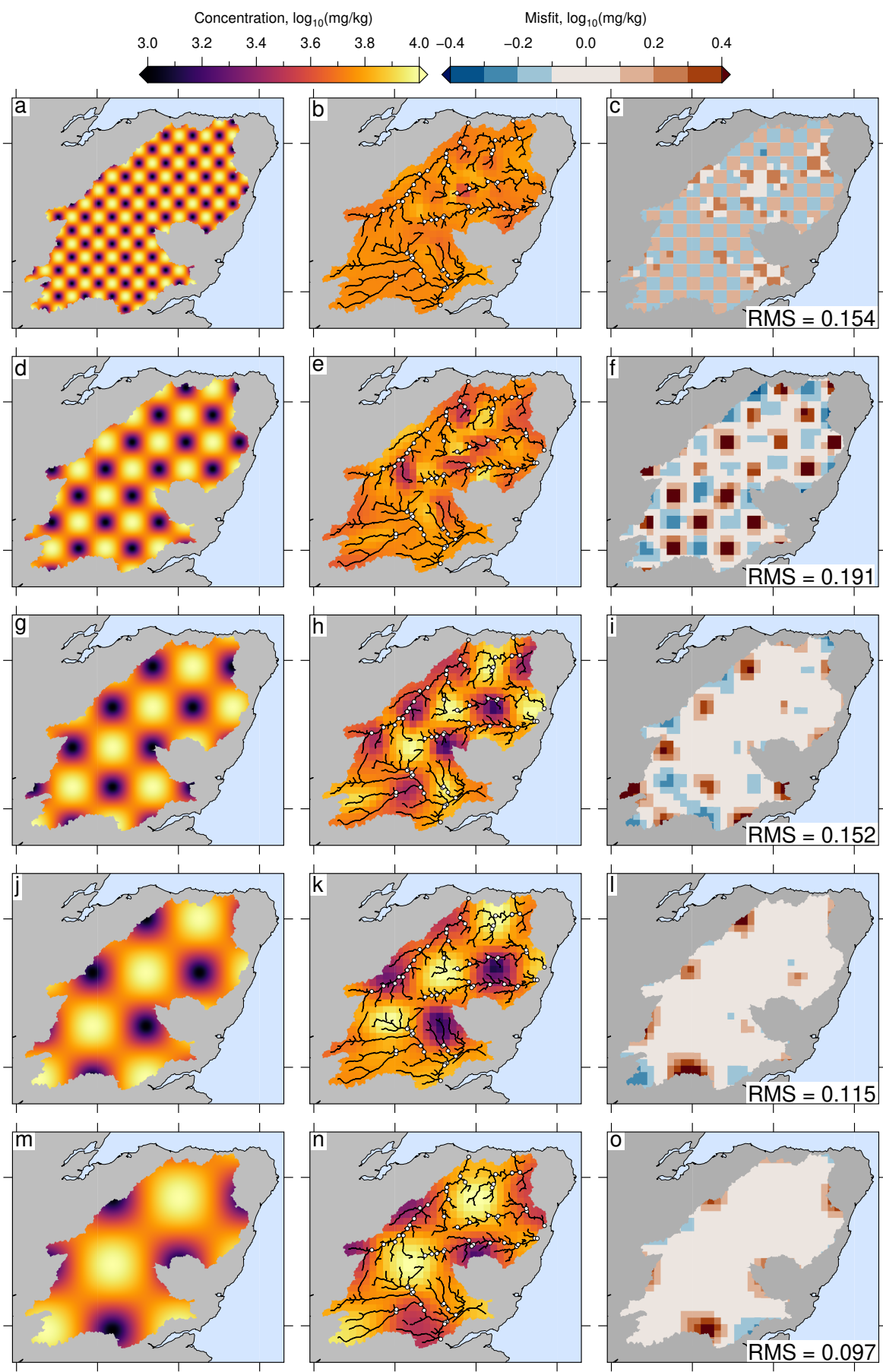
- Figures S1 to S21

Figure S1 shows the results of ‘chequerboard’ tests. In these tests synthetic data at sample sites downstream (e.g. white circles in Figure S1a) are generated using an arbitrary elemental concentration (e.g. Figure S1a). Concentrations at the 67 downstream samples are then inverted for the composition of source regions (see color map in e.g. Figure S1a). These tests are performed using the actual sample sites considered in this study and the real drainage networks in the study region. A comparison between the ‘actual’ source region concentrations and best-fitting results from inverting the 67 sample sites is shown in adjacent panels (e.g. Figure S1c). As discussed in the body text of the main manuscript, changes in source composition at wavelengths < 20 km are poorly

resolved. In contrast, the amplitude and spatial structure of longer wavelength changes in composition are recovered.

Figure S2 shows the results from applying a low-pass (> 25 km) Gaussian filter to the magnesium data extracted from the G-BASE survey, and to the results of the inverse model (see e.g. Figure 13 of the main manuscript). These results are discussed in the main manuscript.

Figure S3–S21 show the results from inverting the elemental concentrations of actual samples for source region chemistry. In the main manuscript we show results for Mg and a subset of results for Ca, Rb, V and Be. Figure S3–21 shows the best-fitting inverse model, the G-BASE inventory and comparisons between these estimates of concentration for Ba, Be, Ca, Co, Cr, Fe, K, La, Li, Mn, Ni, Rb, Sr, Ti, U, V, Y, Zn and Zr. The smoothing parameters for each inverse model were determined by systematically varying λ , the optimum values for each element are given in the captions for Figures S3–21. See body text of the main manuscript for details.



April 15, 2021, 10:29am

Figure S1. Testing the resolution of the inverse model using synthetic examples.

Synthetic inverse problems analogous to that shown in Figures 5–6 of the main manuscript. (a) Synthetic elemental concentration map generated using a 2D sine function with peak to trough = 10 km. This map was used to calculate composition downstream (e.g. at the 67 sample sites shown by white circles in panel b). (b) White circles = sample sites inverted for upstream composition; black curves = rivers with upstream area > 25 km²; colour map = output of best-fitting inverse model. (c) Misfit between maps of ‘observed’ and best-fitting theoretical composition. (d–f) Results when synthetic input has peak-to-trough distance = 20 km. (g–i) Peak-to-trough distance = 30 km. (j–l) Peak-to-trough distance = 40 km (see Figure 5 in main manuscript). (m–o) Peak-to-trough distance = 50 km.

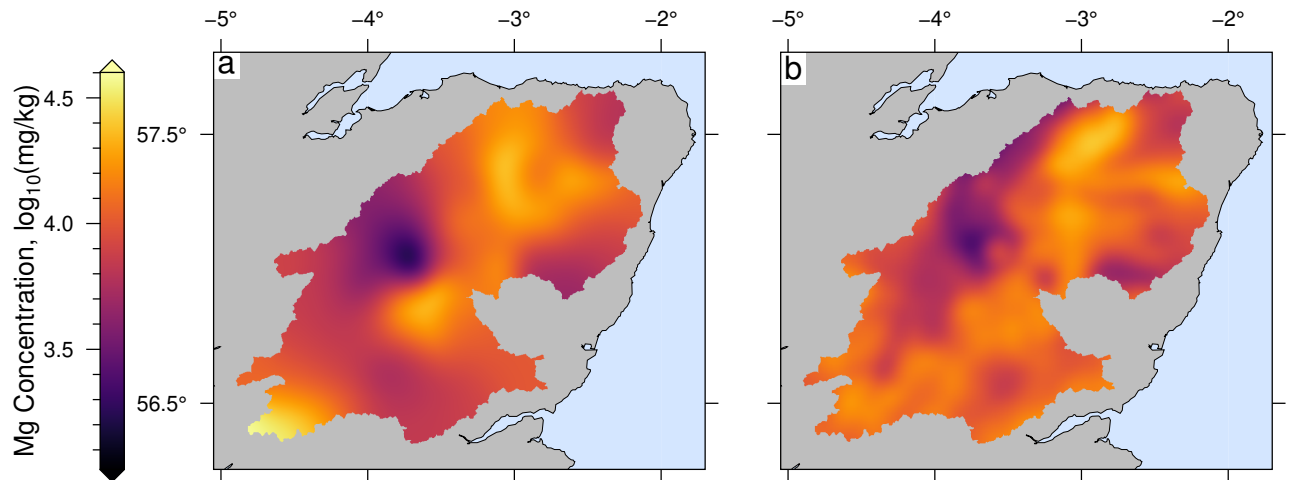


Figure S2. Low-pass filtering of Magnesium. (a) Best-fitting inverse result for Mg filtered using a 2D Gaussian filter of wavelength 25 km. See Figure 7b of the main manuscript for unfiltered results. (b) G-BASE Mg data filtered using same filter as panel (a). Filtered results for other elements are given in Figure 13 of the main manuscript

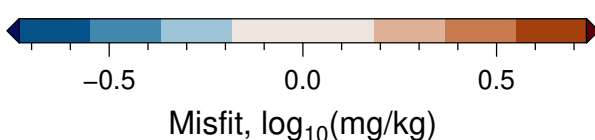
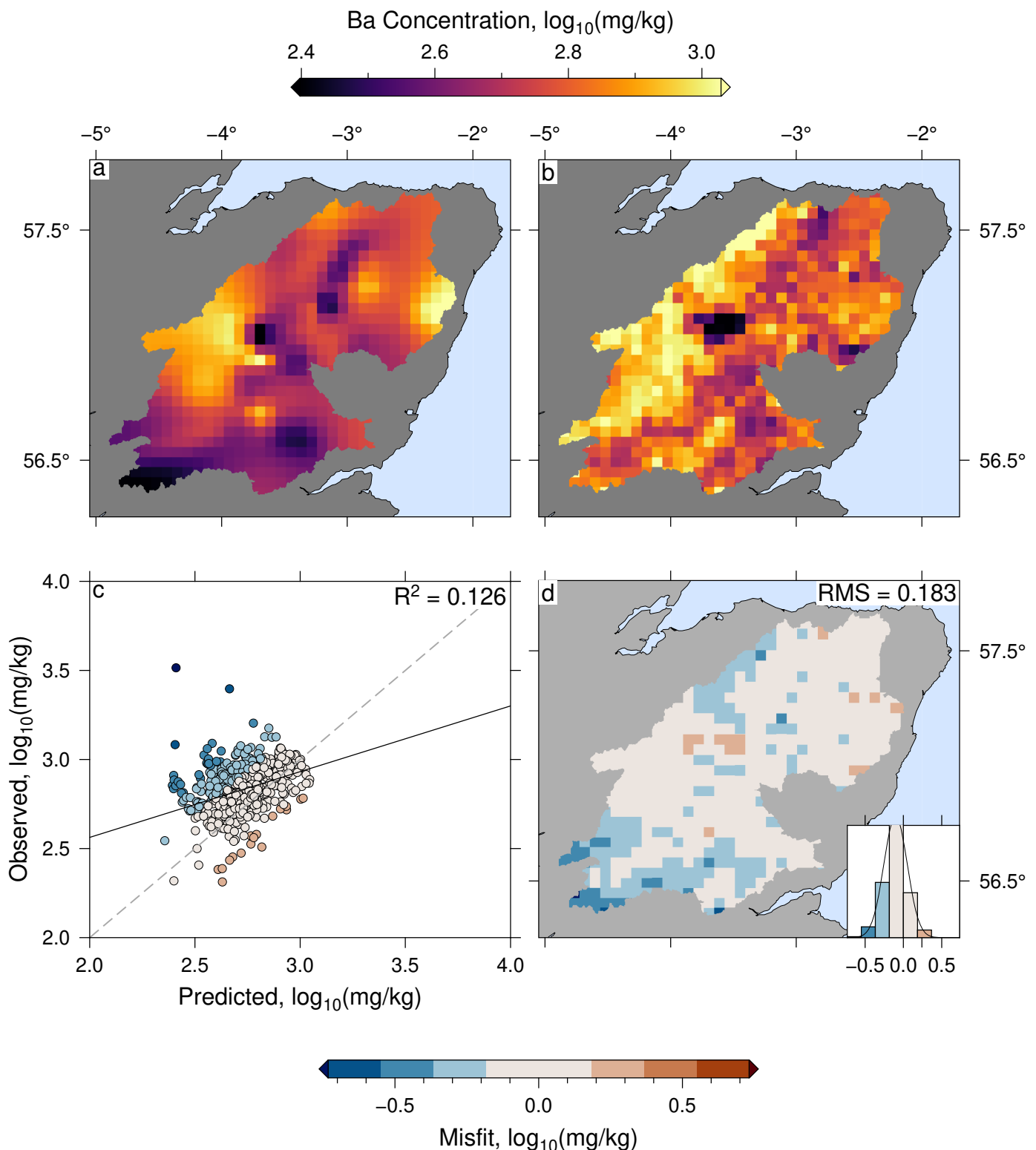


Figure S3. Inverting real downstream sediment samples for concentration of barium in source regions. (a) Optimum upstream concentration of barium generated by inverting the barium concentration of the 67 samples gathered downstream with smoothing parameter $\lambda = 10^{-0.1}$. (b) Independent G-BASE stream sediment concentration of barium gridded to same resolution as panel (a). (c) Cross-plot of observed (G-BASE) and predicted concentrations for each grid cell (5 km resolution). Colors show misfit discretized at intervals equal to global RMS misfit. Gray dashed line = 1:1 relationship; black line = linear regression. (d) Misfit between observed barium concentration and best-fitting inverse model. Inset indicates distribution of residuals and normal distribution; binwidth = global RMS misfit.

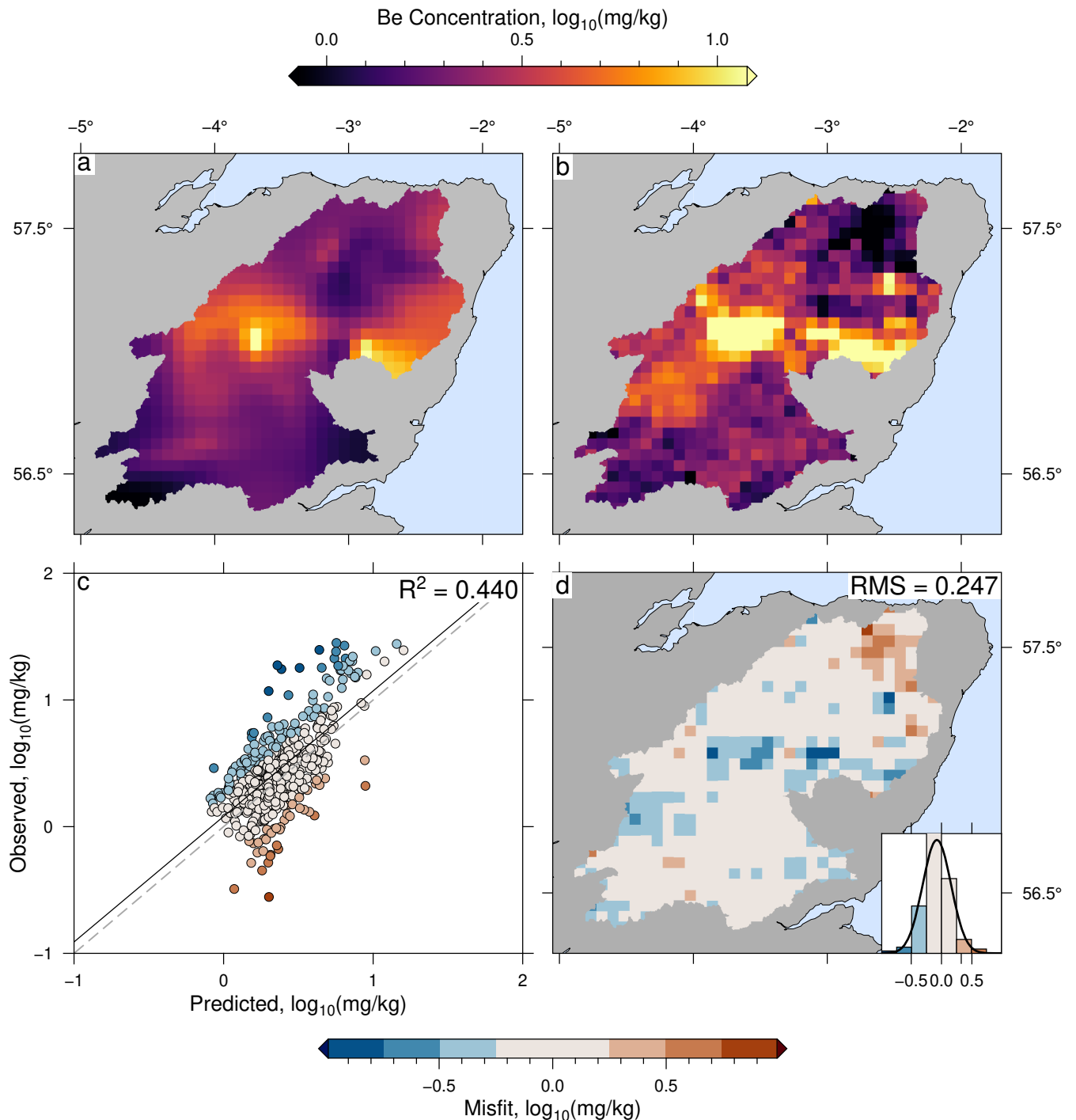


Figure S4. Same as Figure S3 for Be, $\lambda = 10^{0.3}$

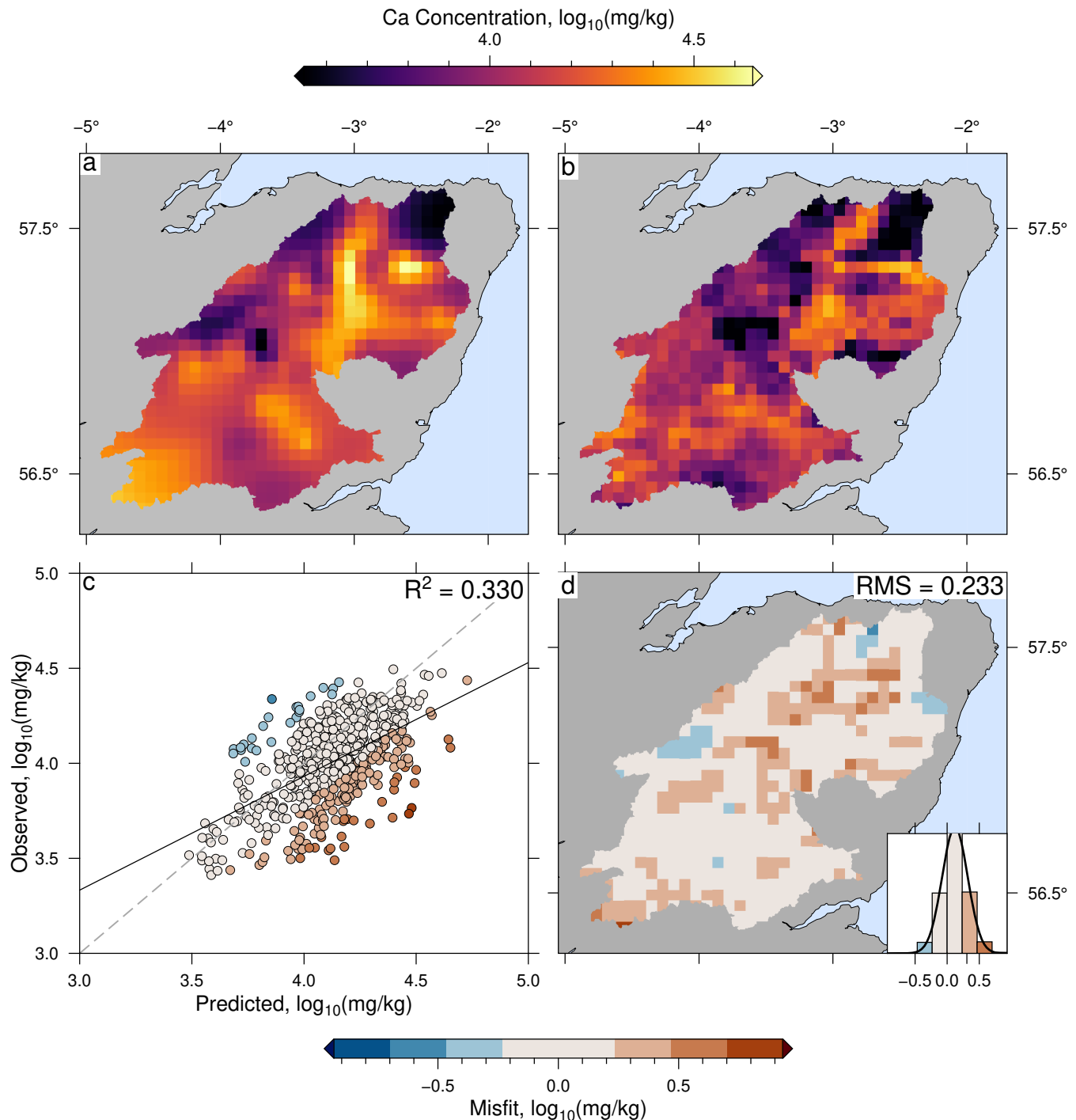


Figure S5. Same as Figure S3 for Ca, $\lambda = 10^{-0.3}$

X - 10

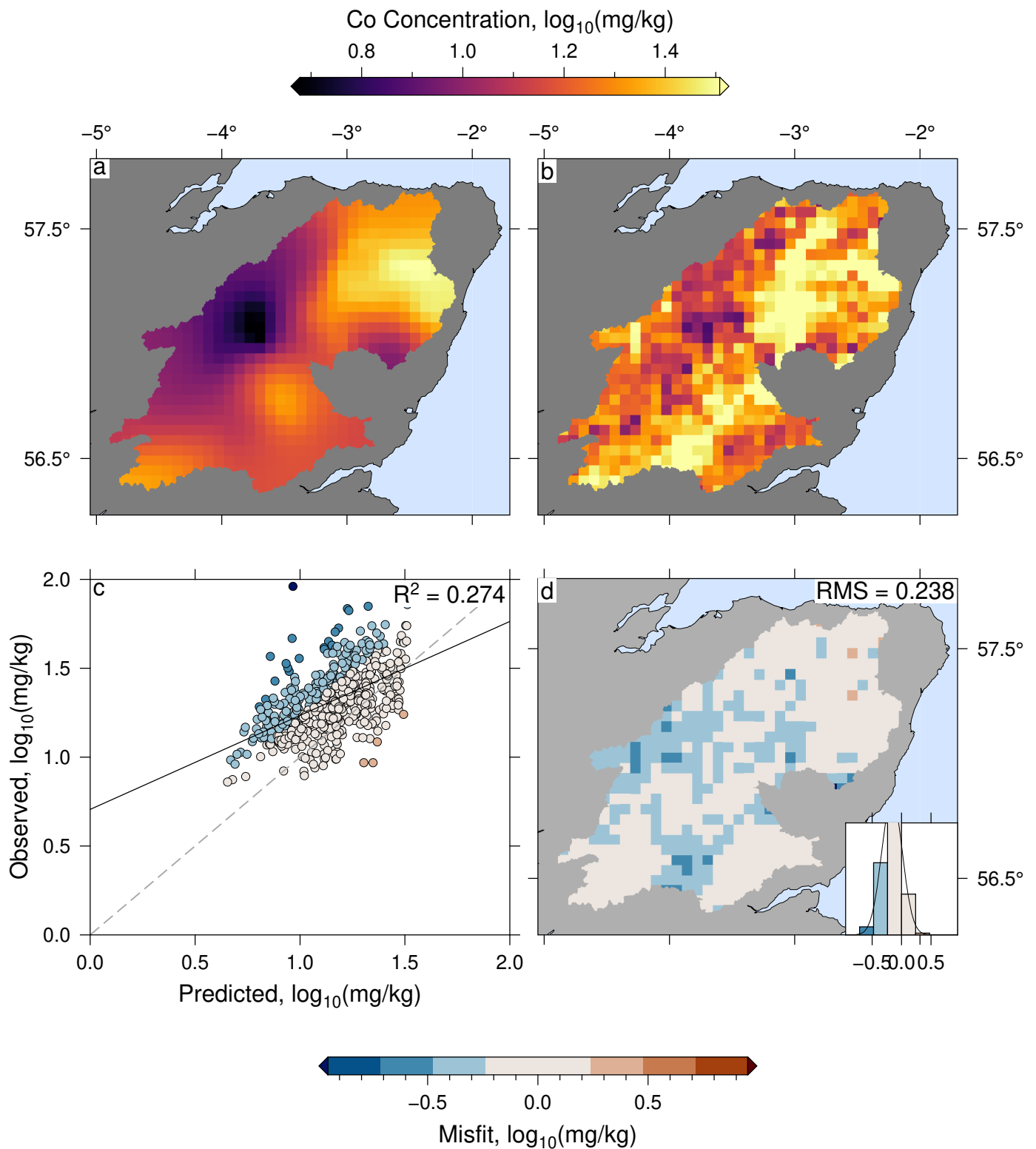


Figure S6. Same as Figure S3 for Co, $\lambda = 10^{0.7}$

April 15, 2021, 10:29am

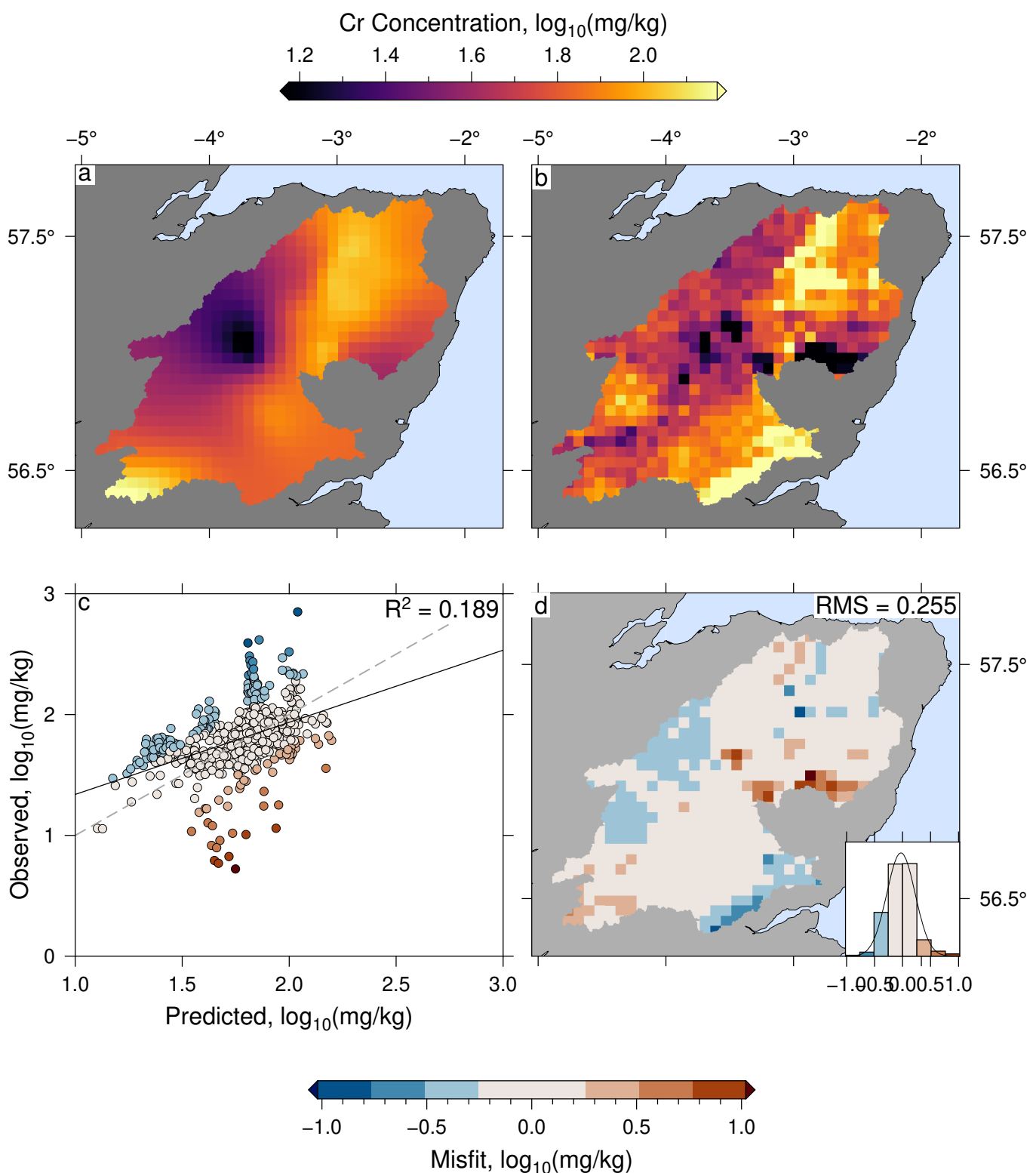


Figure S7. Same as Figure S3 for Cr, $\lambda = 10^{0.8}$

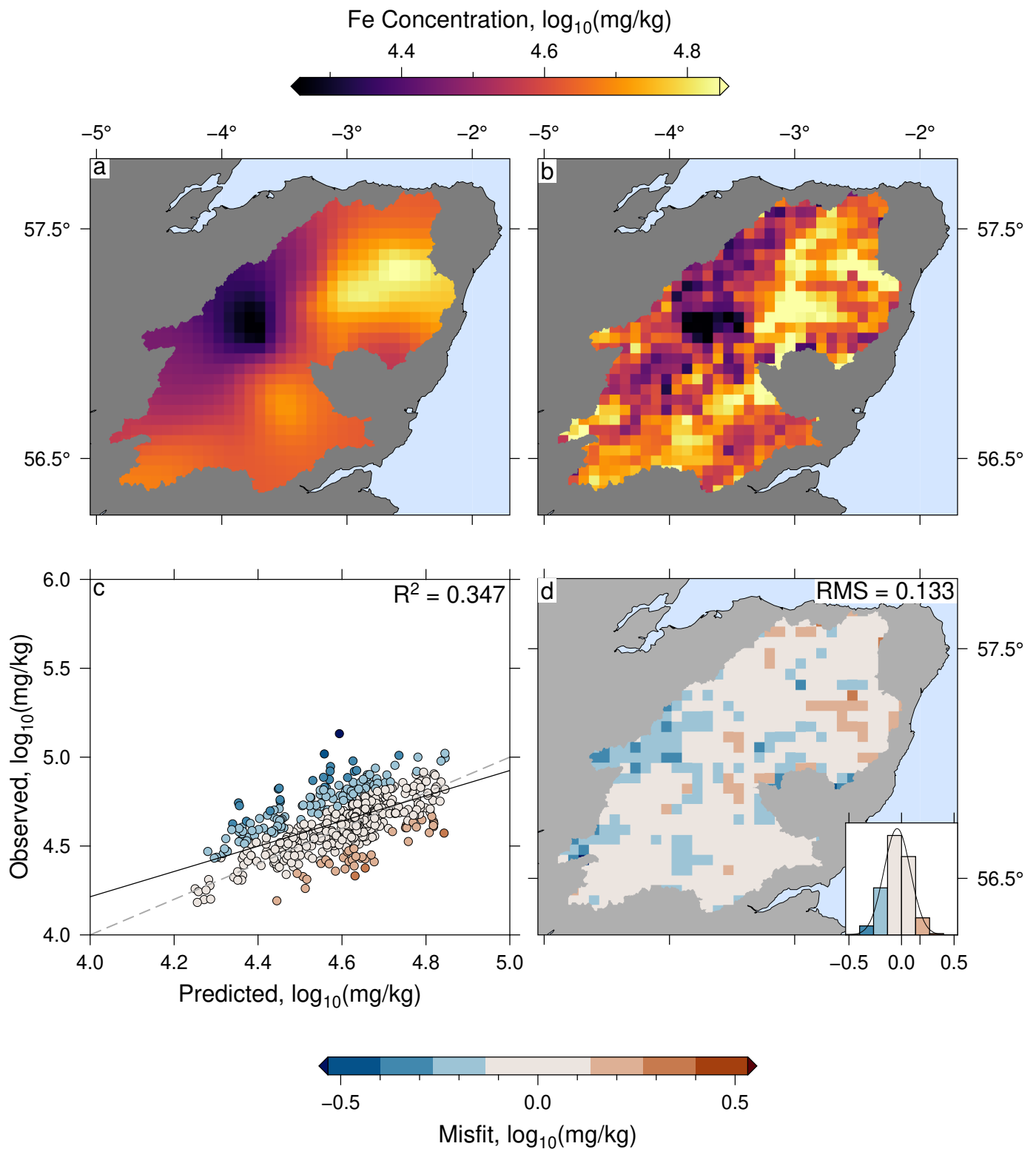


Figure S8. Same as Figure S3 for Fe, $\lambda = 10^{0.8}$

April 15, 2021, 10:29am

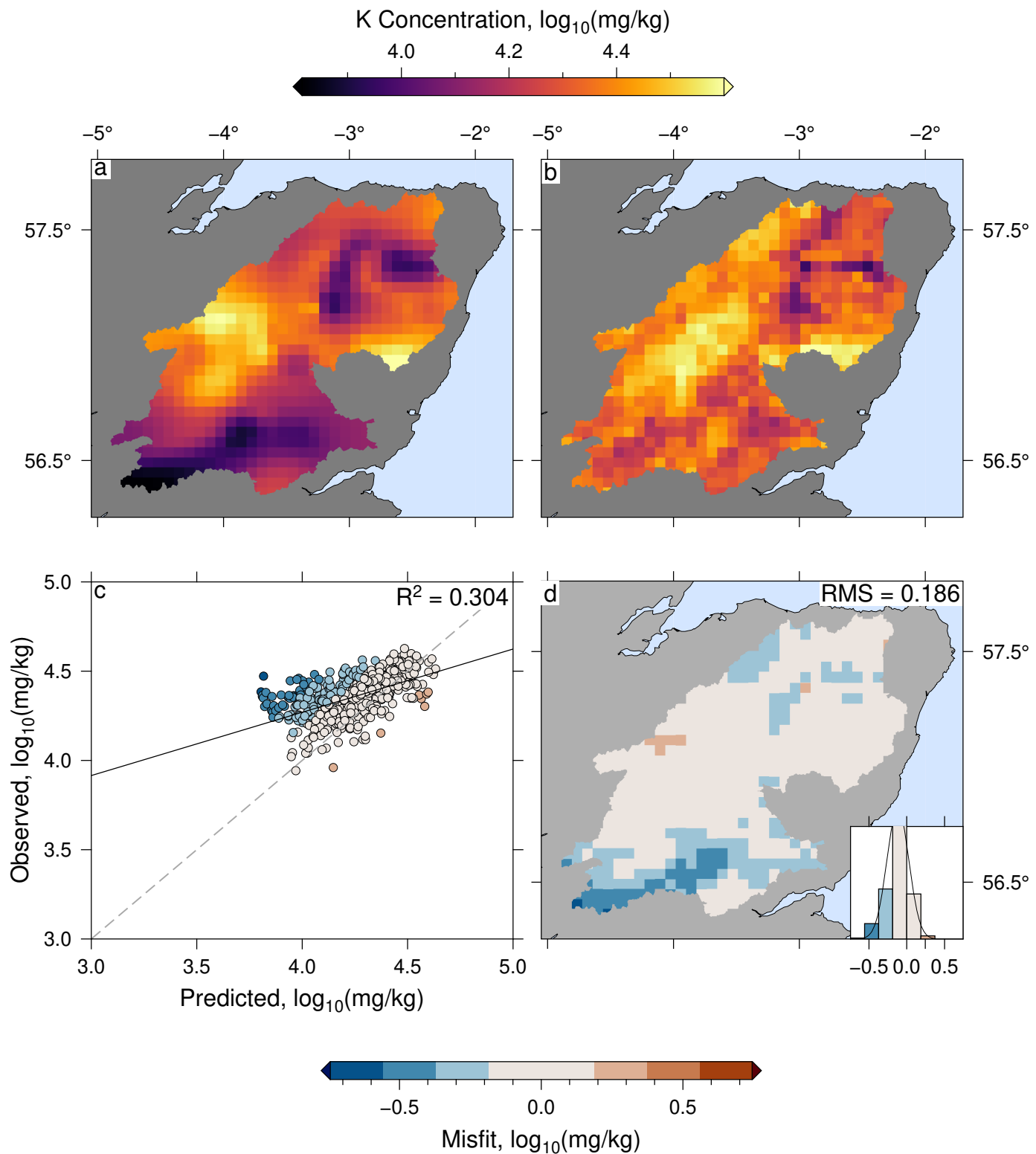


Figure S9. Same as Figure S3 for K, $\lambda = 10^0$

April 15, 2021, 10:29am

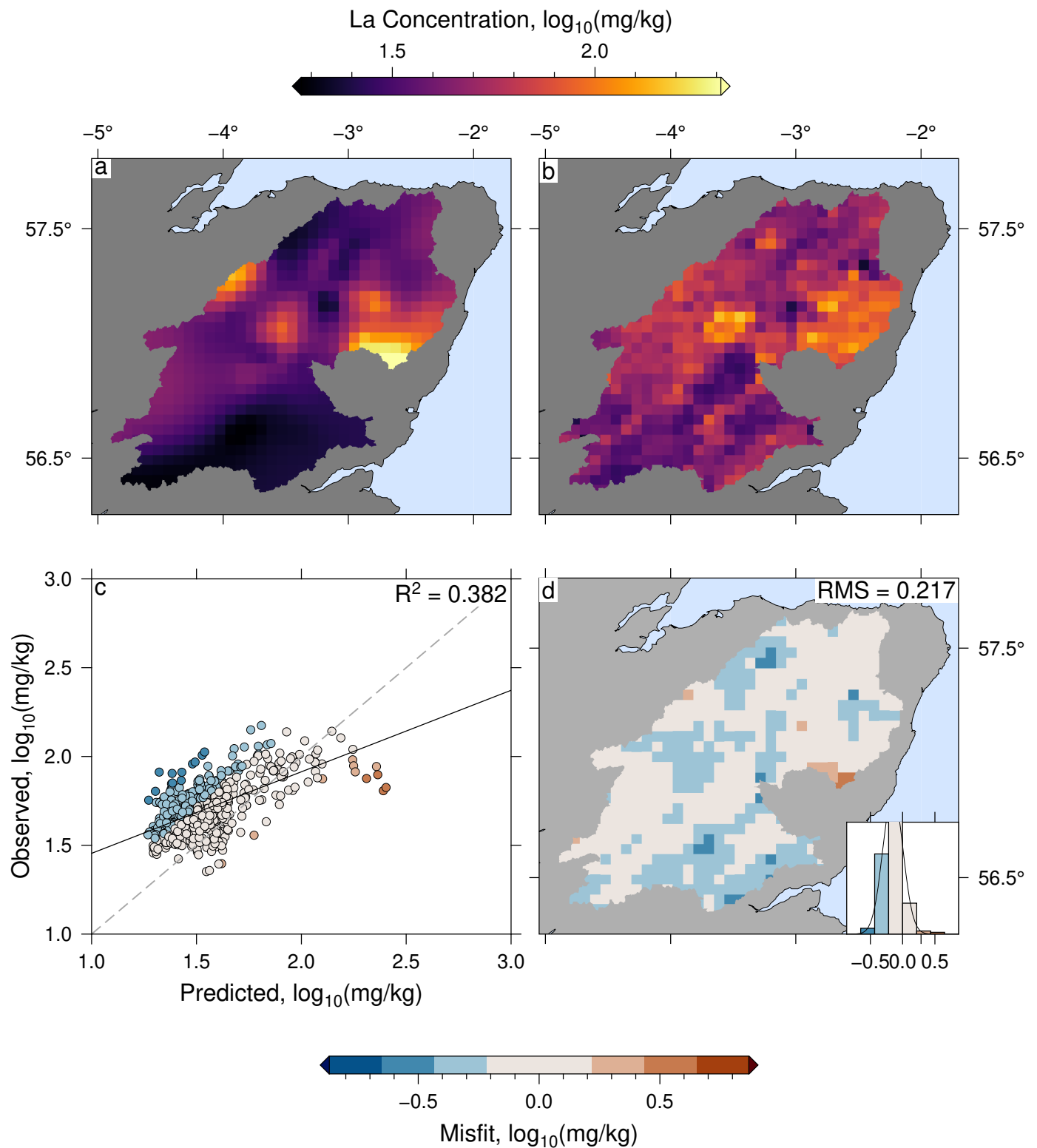


Figure S10. Same as Figure S3 for La, $\lambda = 10^{0.2}$

April 15, 2021, 10:29am

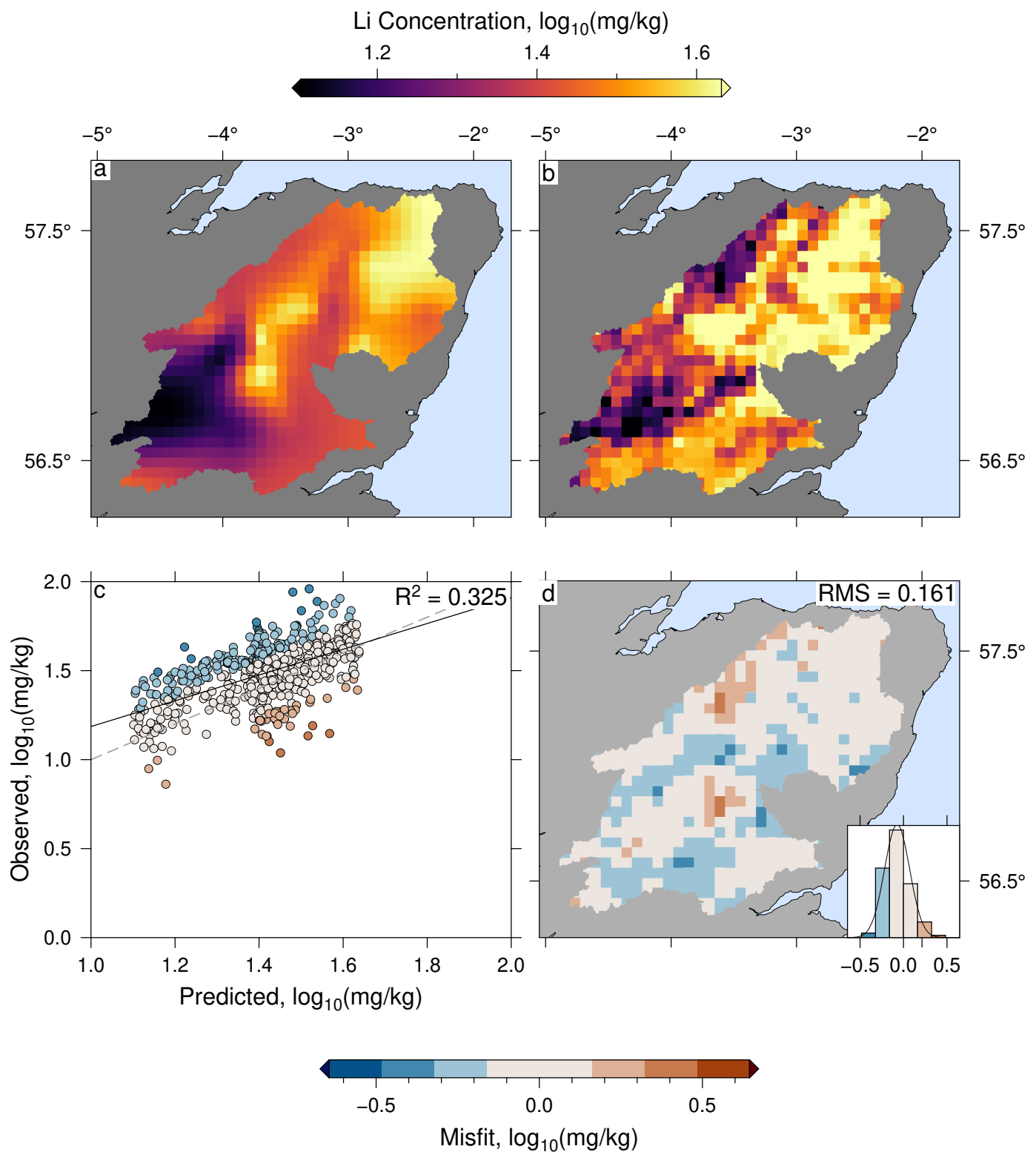


Figure S11. Same as Figure S3 for Li, $\lambda = 10^{0.5}$

April 15, 2021, 10:29am

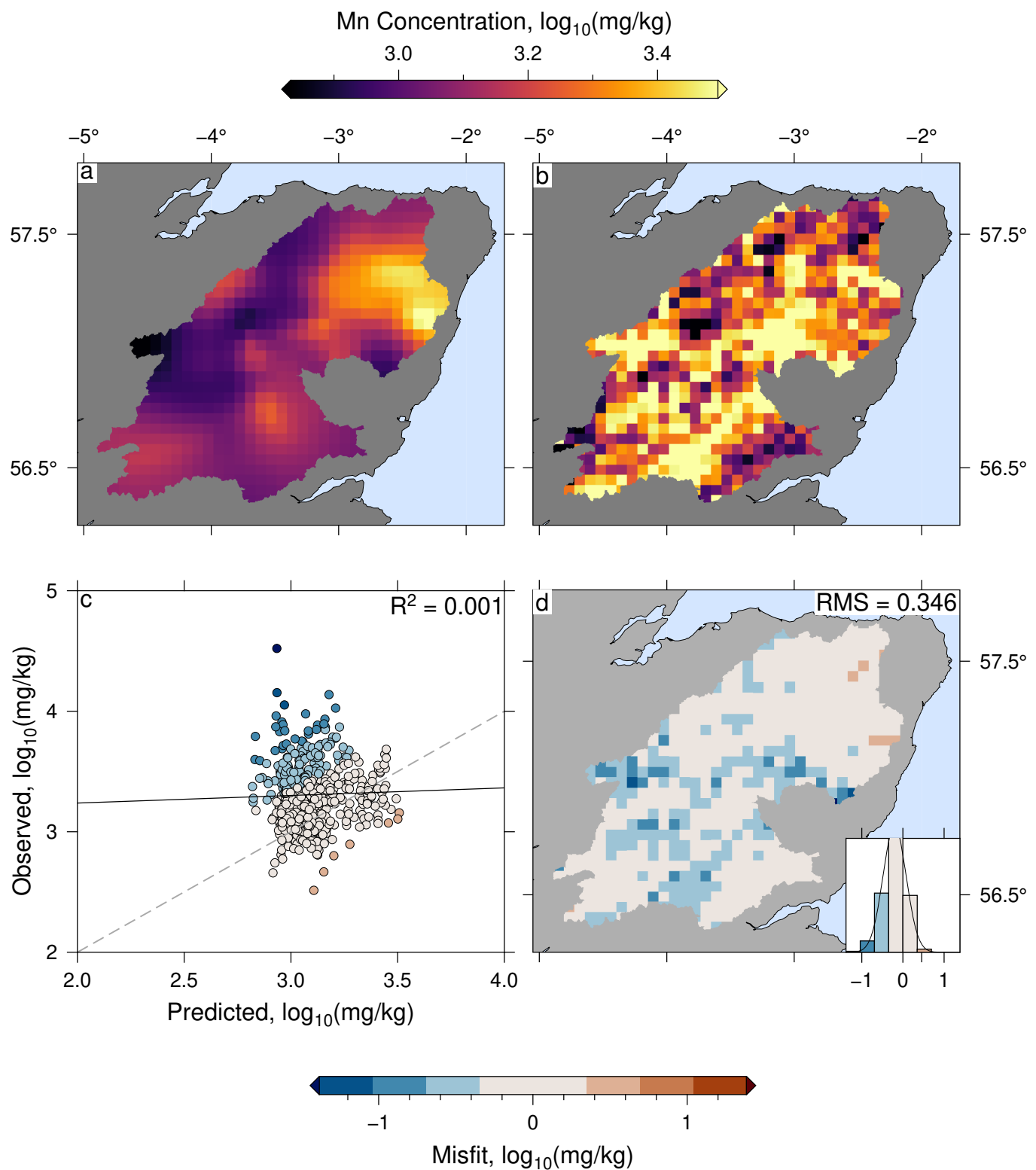


Figure S12. Same as Figure S3 for Mn, $\lambda = 10^{0.7}$

April 15, 2021, 10:29am

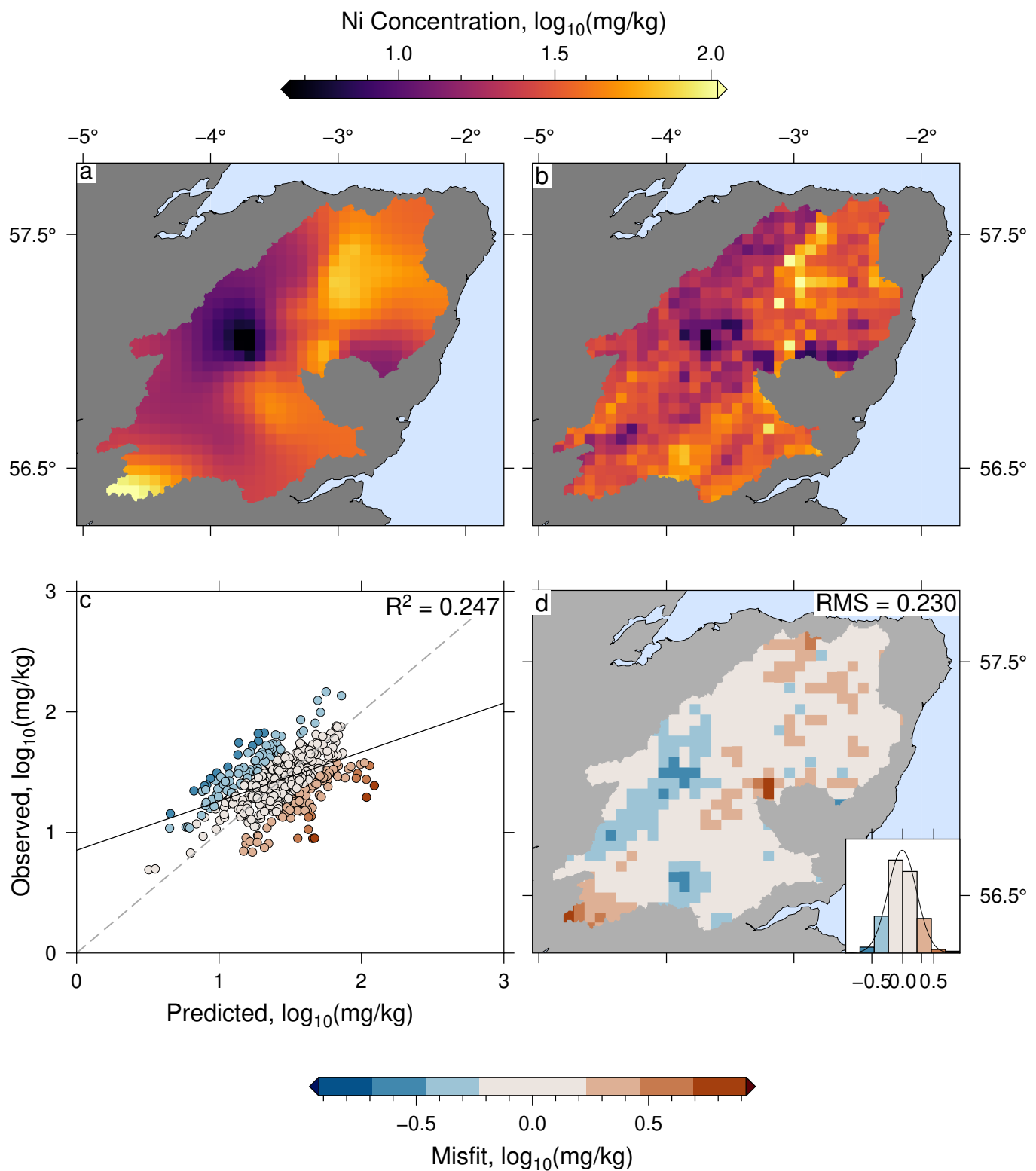


Figure S13. Same as Figure S3 for Ni, $\lambda = 10^{0.5}$

April 15, 2021, 10:29am

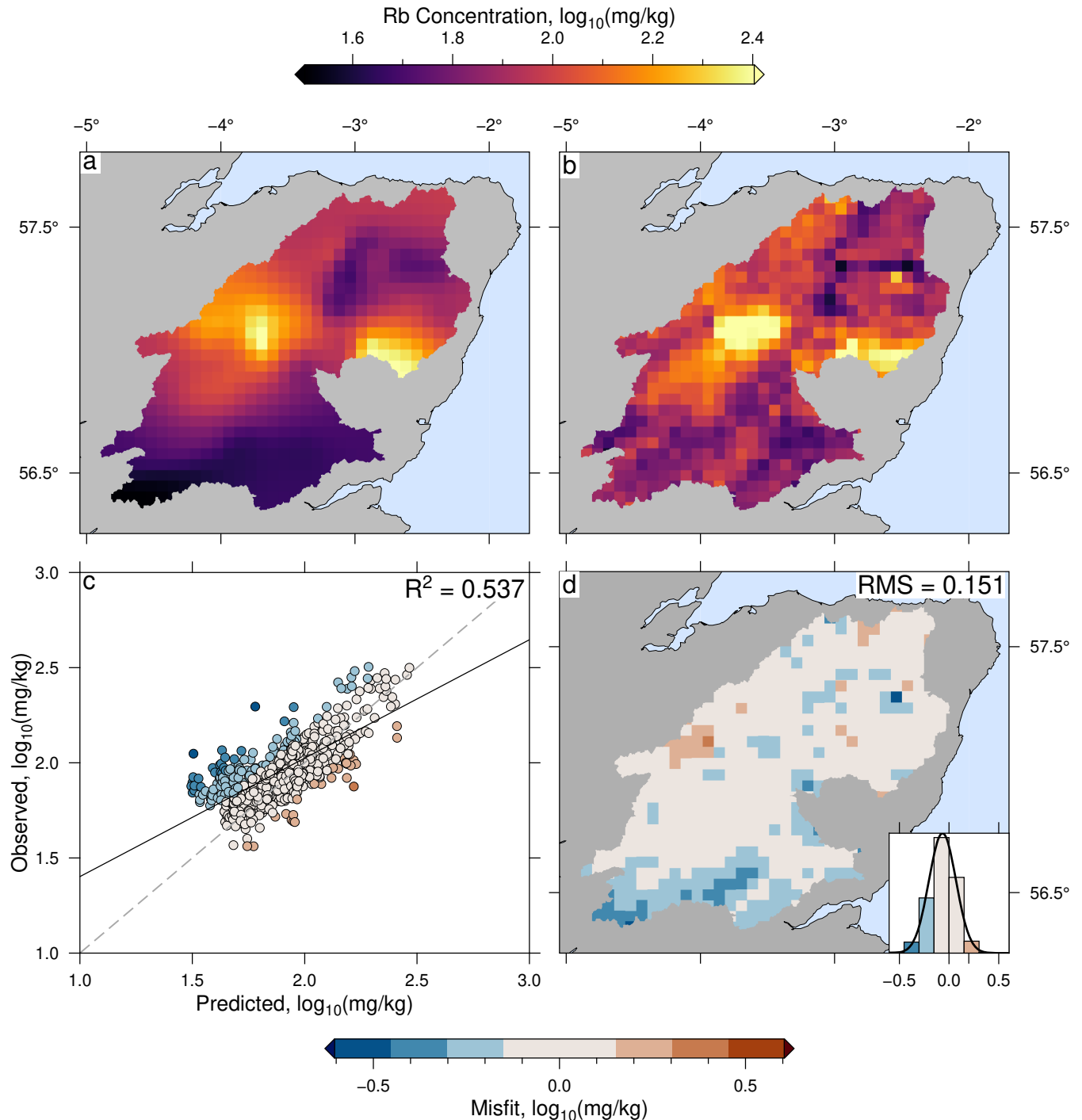


Figure S14. Same as Figure S3 for Rb, $\lambda = 10^{0.4}$

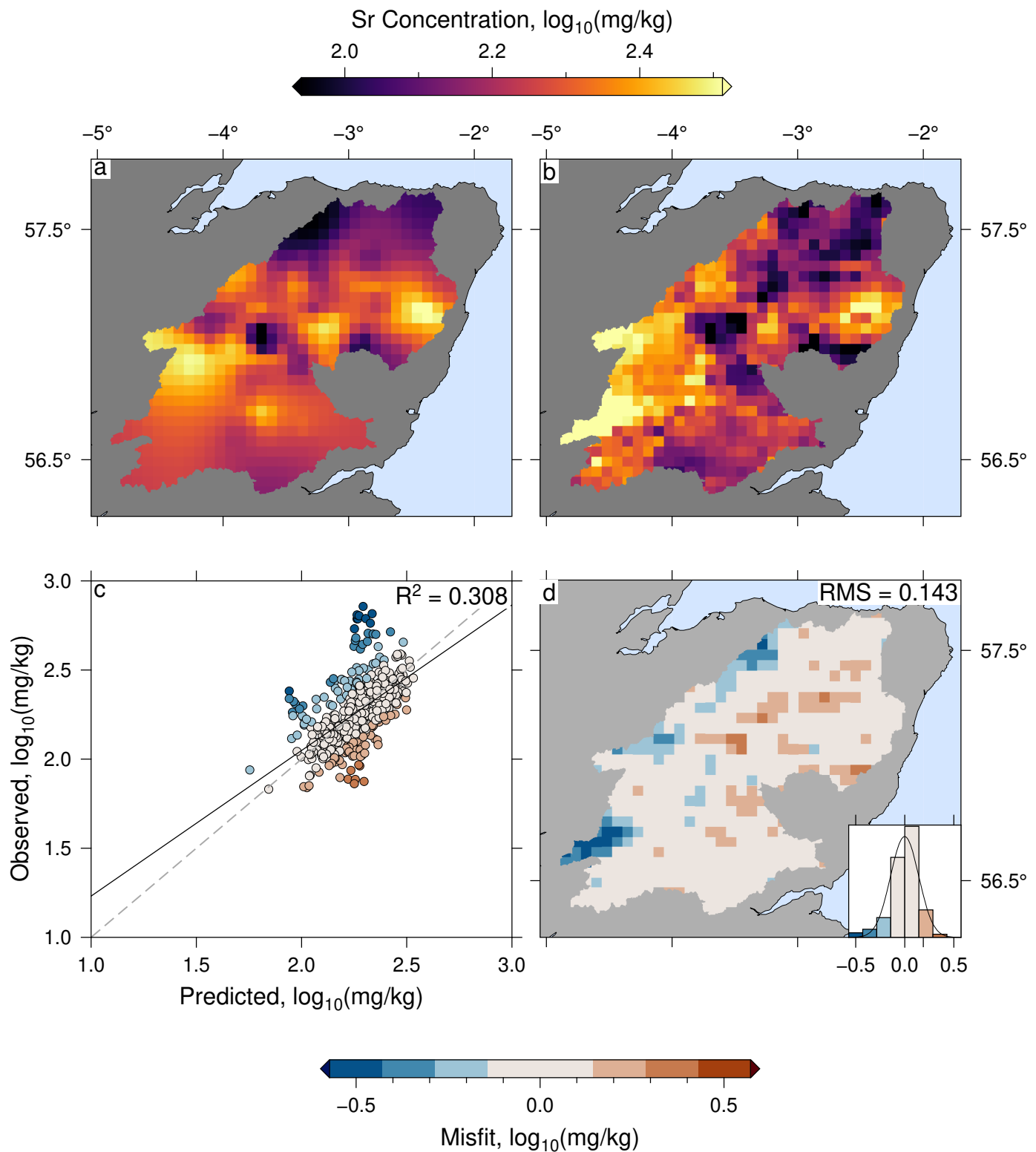


Figure S15. Same as Figure S3 for Sr, $\lambda = 10^{-0.1}$

April 15, 2021, 10:29am

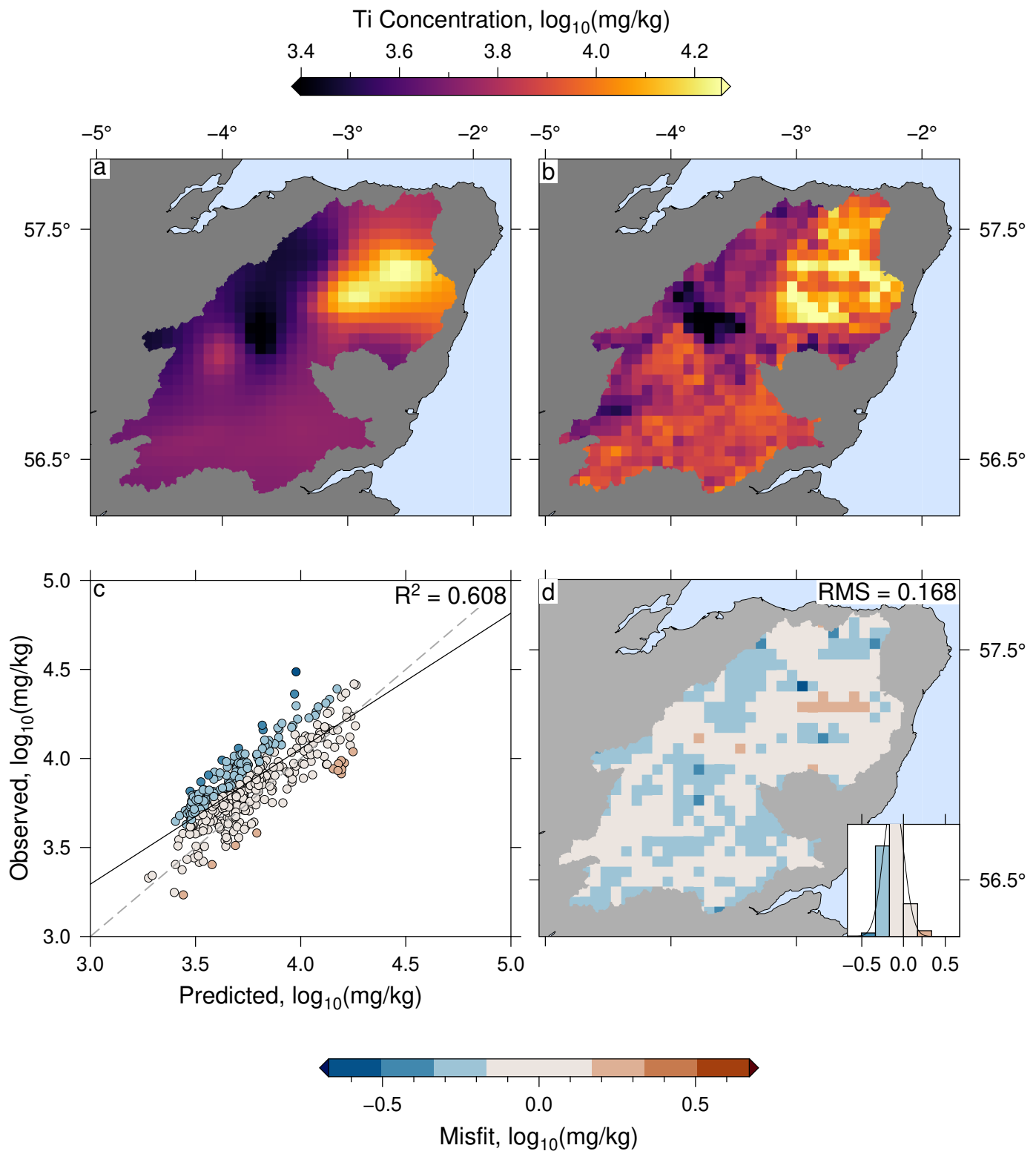


Figure S16. Same as Figure S3 for Sr, $\lambda = 10^{0.7}$

April 15, 2021, 10:29am

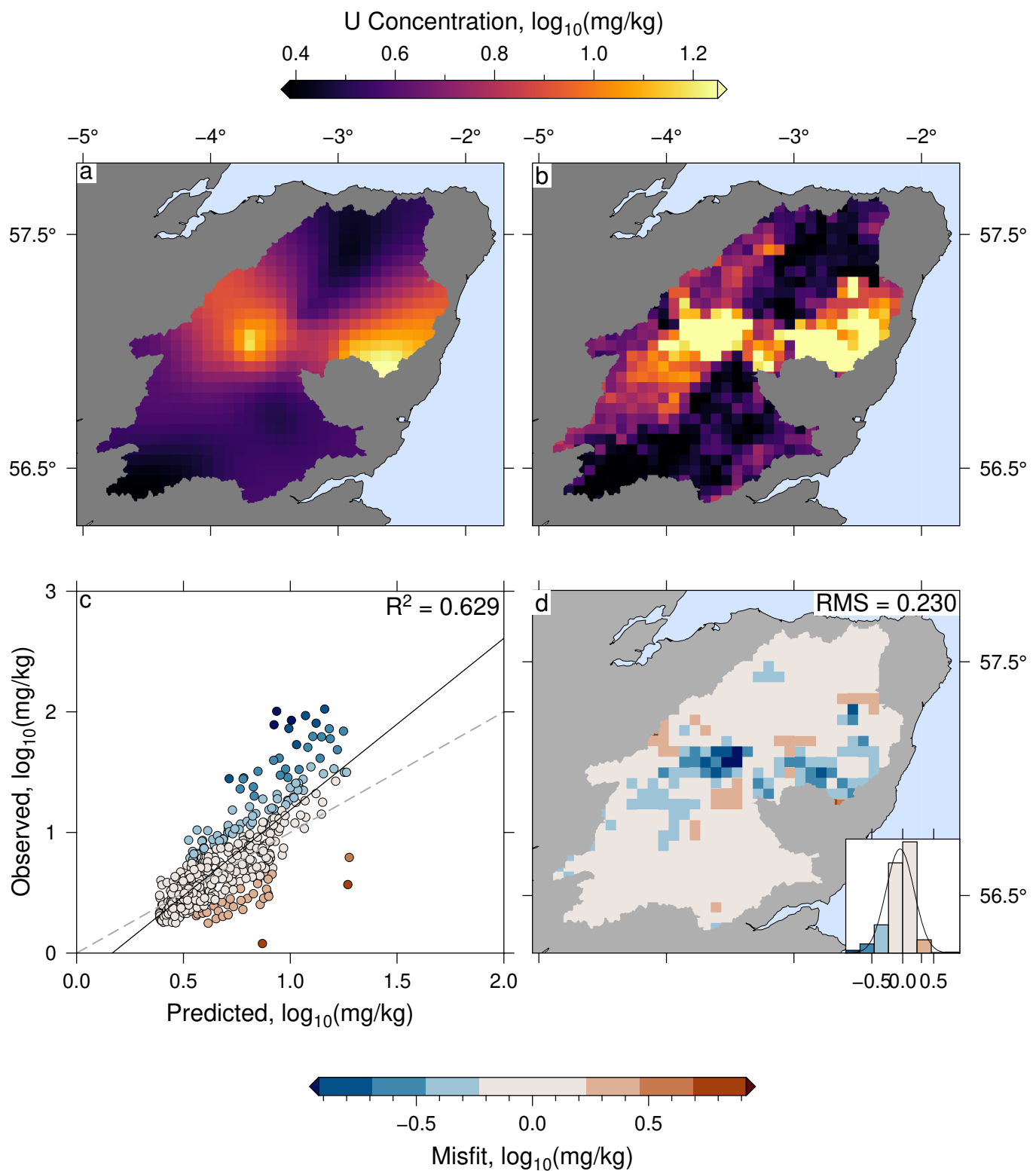


Figure S17. Same as Figure S3 for U, $\lambda = 10^{1.0}$

April 15, 2021, 10:29am

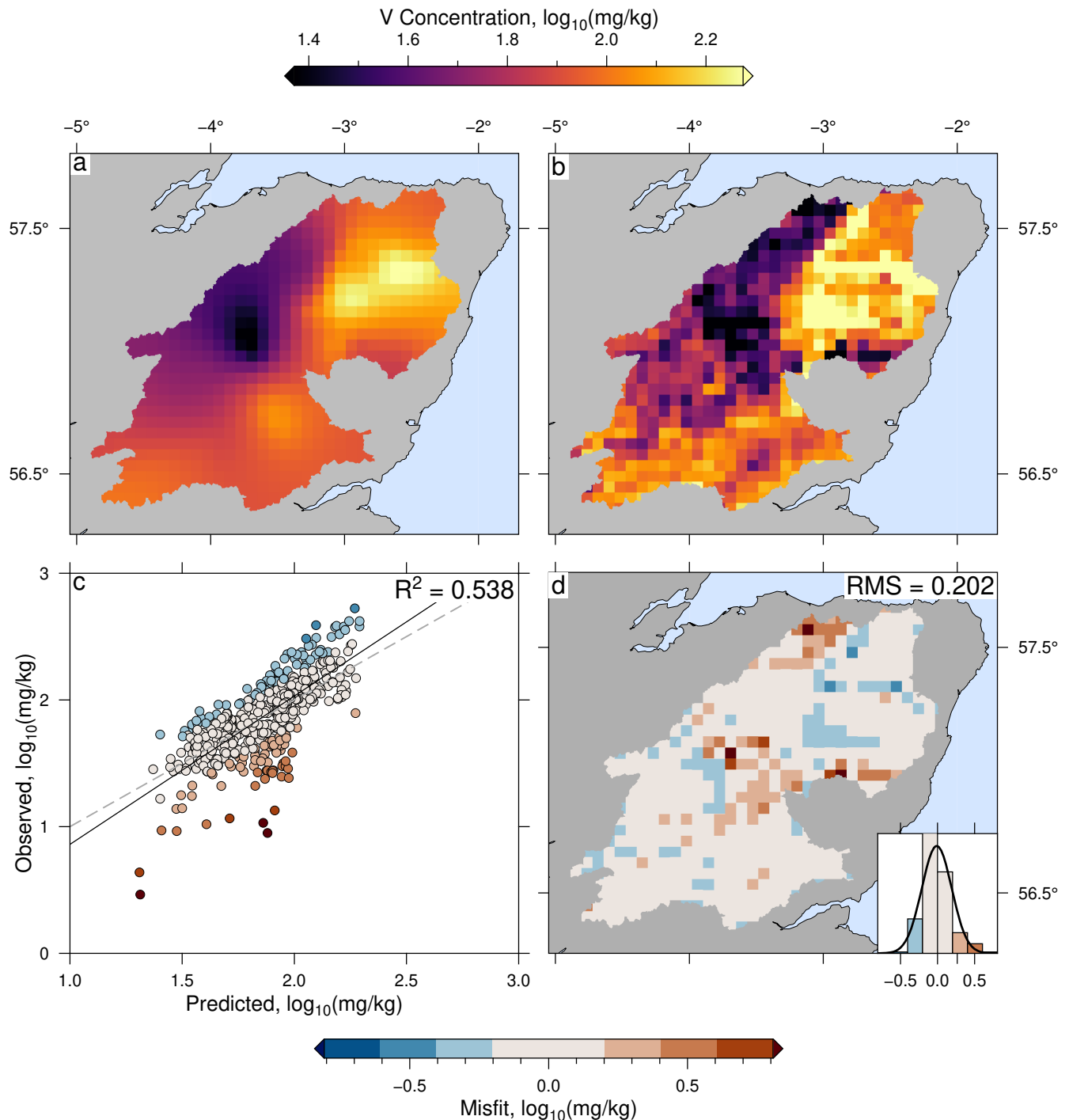


Figure S18. Same as Figure S3 for V, $\lambda = 10^{0.7}$

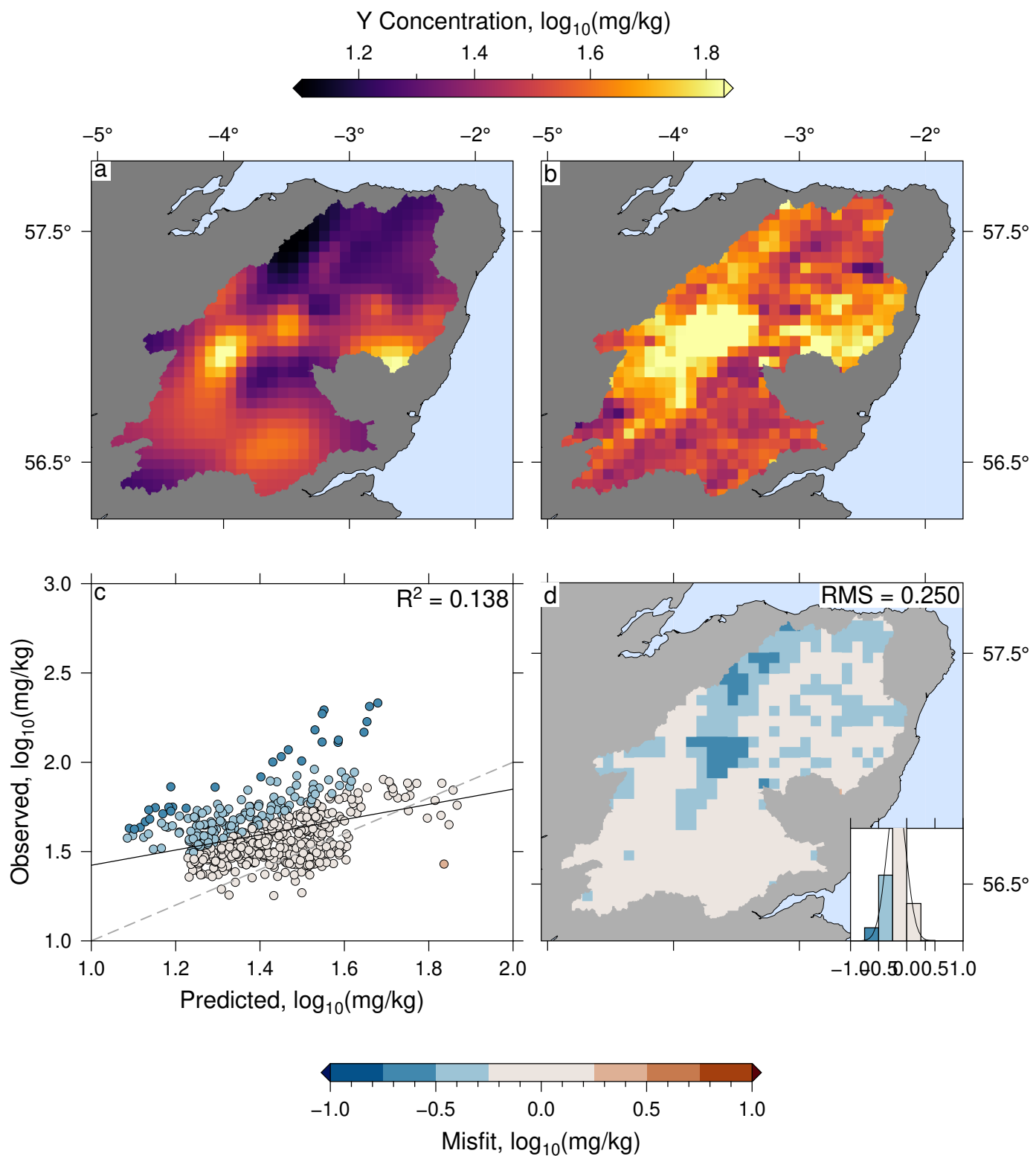


Figure S19. Same as Figure S3 for Y, $\lambda = 10^{0.2}$

April 15, 2021, 10:29am

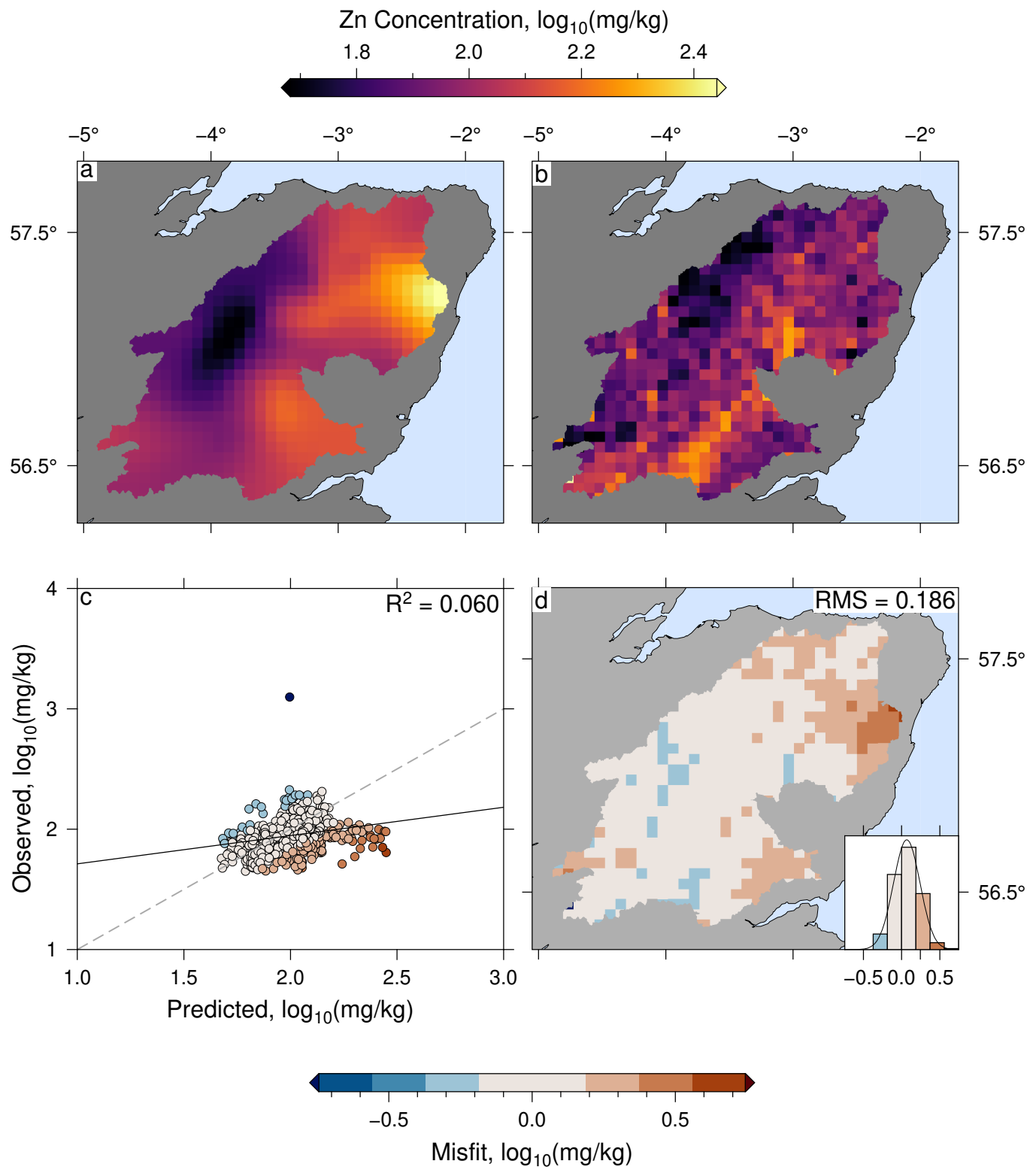


Figure S20. Same as Figure S3 for Zn, $\lambda = 10^{0.6}$

April 15, 2021, 10:29am

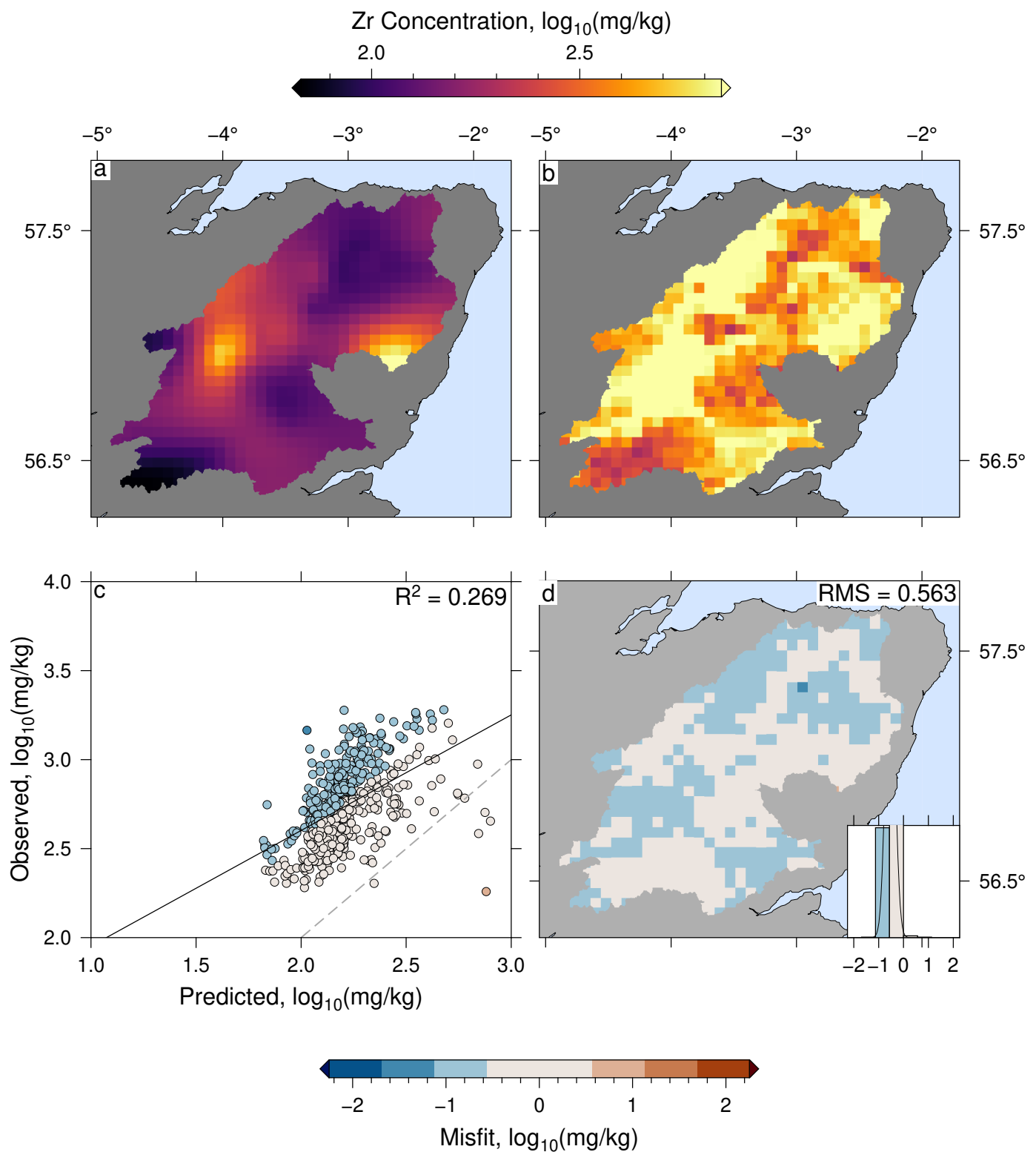


Figure S21. Same as Figure S3 for Zr, $\lambda = 10^{0.7}$

April 15, 2021, 10:29am